MOLECULAR AND CELLULAR BIOLOGY, May 2004, p. 4417–4427 Vol. 24, No. 10
0270-7306/04/$08.00+0 DOI: 10.1128/MCB.24.10.4417–4427.2004

The Transcription Factor RFX3 Directs Nodal Cilium Development and Left-Right Asymmetry Specification

E. Bonnafe,[1] M. Touka,[1] A. AitLounis,[2] D. Baas,[1]† E. Barras,[2] C. Ucla,[2]‡ A. Moreau,[3] F. Flamant,[4] R. Dubruille,[1] P. Couble,[1] J. Collignon,[3] B. Durand,[1]§* and W. Reith[2]§*

Centre de Génétique Moléculaire et Cellulaire, CNRS UMR 5534, Université Claude Bernard Lyon-1, F-69622 Villeurbanne,[1] Laboratoire de Biologie Moléculaire et Cellulaire, CNRS UMR 49, ENSL, F-69364 Lyon,[4] and Departement de Biologie du Développement, Institut Jacques-Monod, CNRS UMR, Université Paris 6-7, F-75251 Paris,[3] France, and Department of Pathology, University of Geneva Medical School, CMU, CH-1211 Geneva, Switzerland[2]

Received 8 September 2003/Returned for modification 27 October 2003/Accepted 6 February 2004

There are five members of the RFX family of transcription factors in mammals. While RFX5 plays a well-defined role in the immune system, the functions of RFX1 to RFX4 remain largely unknown. We have generated mice with a deletion of the *Rfx3* gene. RFX3-deficient mice exhibit frequent left-right (LR) asymmetry defects leading to a high rate of embryonic lethality and situs inversus in surviving adults. In vertebrates, specification of the LR body axis is controlled by monocilia in the embryonic node, and defects in nodal cilia consequently result in abnormal LR patterning. Consistent with this, *Rfx3* is expressed in ciliated cells of the node and RFX3-deficient mice exhibit a pronounced defect in nodal cilia. In contrast to the case for wild-type embryos, for which we document for the first time a twofold increase in the length of nodal cilia during development, the cilia are present but remain markedly stunted in mutant embryos. Finally, we show that RFX3 regulates the expression of *D2lic*, the mouse orthologue of a *Caenorhabditis elegans* gene that is implicated in intraflagellar transport, a process required for the assembly and maintenance of cilia. In conclusion, RFX3 is essential for the differentiation of nodal monocilia and hence for LR body axis determination.

Vertebrates display a conserved asymmetric pattern of distribution of the visceral organs along the left-right (LR) body axis. Molecular and genetic studies performed with the chicken, frog, zebra fish, and mouse systems have shown that laterality decisions are mediated by a cascade of genes that function at the late gastrulation and early somite stages (for a review, see reference 16). It is well known that this pathway leads to the asymmetric expression of genes such as *nodal*, *lefta*/*Ebaf*, *leftb*, and *pitx2* in the lateral plate mesoderm. However, the mechanisms causing the initial break in LR symmetry are less well understood. It has become clear in recent years that ciliated cells of the embryonic node play a crucial role in the breaking of LR symmetry in the mouse (32; reviewed in references 4 and 26). Ciliated embryonic cells similar to those of the mouse node are found across a wide range of vertebrates, suggesting that the involvement of cilia in breaking bilateral symmetry is universal in vertebrate development (11). This is consistent with the fact that there is also a link between the motility of cilia and the regulation of LR asymmetry in humans. Patients with Kartagener syndrome have a mirror image reversal in the LR orientation of their internal organs (situs inversus), together with respiratory difficulties caused by immotile tracheal cilia and male infertility related to defects in sperm motility. For certain patients, this syndrome has been shown to result from mutations in the components of ciliary motors (1, 15, 19, 35, 38).

Although the implication of nodal cilia in LR determination is now well established, the precise mechanisms involved are less well defined. The movement of monocilia in the node generates a leftward flow that subsequently induces the nodal pathway in the lateral plate mesoderm (32, 34). The artificial reversal of this flow induces laterality defects (31). It has therefore been proposed that the unidirectional flow driven by the nodal cilia generates a morphogen concentration gradient that triggers asymmetric gene expression via an unknown mechanism. More recently, it was shown that monocilia of the node can exert two functions, namely the generation of a nodal flow and the mechanosensation of this flow, leading to an asymmetric calcium signaling cascade in the node itself (27).

Cilia are well-defined structures consisting of a microtubular axoneme composed of specific proteins that are assembled dynamically in a strict stereotypical pattern. These proteins are strongly conserved in organisms ranging from the green algae *Chlamydomonas* to mammals. Functional studies using various organisms have been instrumental in the identification of genes involved in the assembly and function of cilia. Cilia are assembled via a process called intraflagellar transport (IFT). IFT is a process in which large protein assemblies, called IFT particles or rafts, are conveyed to the distal tip of flagella by the heterotrimeric kinesin II complex and are brought back to the

* Corresponding author. Mailing address for B. Durand: Centre de Génétique Moléculaire et Cellulaire, CNRS UMR 5534, Université Claude Bernard, 43 Bvd. du 11 Novembre 1918, F-69622 Villeurbanne, France. Phone: 0033 4 72 44 62 60. Fax: 0033 4 72 44 05 55. E-mail: Benedicte.Durand@univ-lyon1.fr. Mailing address for W. Reith: Department of Pathology, University of Geneva Medical School, CMU, 1 rue Michel-Servet, CH-1211 Geneva, Switzerland. Phone: 0041 22 379 56 66. Fax: 0041 22 379 57 46. E-mail: Walter.Reith@medecine.unige.ch.

§ B.D. and W.R. contributed equally to this work.

† Present address: IBCP, F-69367 Lyon, France.

‡ Present address: Division of Medical Genetics, University of Geneva Medical School, CMU, CH-1211 Geneva, Switzerland.

base by a cytoplasmic dynein complex (reviewed in references 45 and 52). IFT was first described for *Chlamydomonas* and was subsequently found to be essential for the assembly and maintenance of sensory cilia in *Caenorhabditis elegans* and of primary and motile cilia in mice (6, 23, 36). IFT particles are composed of at least 17 polypeptides assembled in two complexes, called A and B, and several conserved IFT raft proteins have been identified. For instance, IFT88/OSM-5/TG737 has been shown to play an important role in IFT in *Chlamydomonas*, *C. elegans*, and mice (18, 36, 41). Similarly, XBX-1/DLIC functions in IFT in *C. elegans* and *Chlamydomonas* (40, 48).

In the mouse, mutations in several genes required for the formation, integrity, or functioning of cilia give rise to defects in the determination of the asymmetric LR body axis. These genes can be classified into three groups. The first set of genes is required for the assembly of monocilia in the embryonic node. This group includes, for example, the genes encoding the kinesin subunits KIF3A and KIF3B (25, 32) and the gene (*Tg737*) encoding the IFT raft protein Polaris (29). The second group of genes encode proteins required for movement of the nodal monocilia. The inversus viscerum (*iv*) mouse is deficient in left-right dynein (Lrd). *iv* mice have immotile nodal cilia and lack any discernible flow in the node region (54). In the *inv* mouse, nodal monocilia are present and motile, but their movement is slower than normal (34). The function of the protein encoded by the *inv* gene is unknown, but it is a component of various primary cilia (59). This second group probably also includes the genes encoding DNA polymerase lambda and HFH-4 (3, 5, 22). The third group includes genes that do not play known roles in the assembly or movement of cilia and may fulfill other functions, such as a sensory function, in the nodal monocilia. Mice deficient in the *Pkd2* gene apparently have normal nodal cilia, yet they have a randomization of LR asymmetry (39). *Pkd2* encodes a transmembrane protein that has Ca^{2+} channel activity and interacts with polycystine 1, a large protein with receptor-like properties (30, 61). Polycystins are likely candidates for generating the asymmetric calcium signal observed in the node in response to nodal flow (27).

The descriptions of the above-mentioned mouse mutants emphasize the fact that the genetic dissection of cilium formation and function is central to our understanding of the mechanisms underlying LR asymmetry specification. Surprisingly, however, very little is known about the regulatory pathways that control the expression of cilium components or direct the differentiation of cilia in vertebrates. Genetic studies with *C. elegans* and *Drosophila melanogaster* have shown that the transcription factors DAF-19 and dRFX are involved in sensory cilium specification (9, 55). DAF-19 and dRFX belong to the RFX family, which is defined by a characteristic DNA binding domain with a structure that is related to the winged-helix subfamily of helix-turn-helix domains (10, 12, 42, 44). So far, all of the DAF-19 target genes identified and characterized in *C. elegans* are involved in IFT (17, 18, 48, 55). A number of genes regulated by dRFX in *D. melanogaster* are homologues of DAF-19 target genes (R. Dubruille and B. Durand, unpublished data). Taken together, these results suggest that RFX factors have conserved a pivotal role in controlling cilium formation in different species.

In mammals, there are five members of the RFX family (10). RFX5 is the only member for which the function is well defined: it plays a pivotal regulatory role in the immune system (53; reviewed in reference 43). RFX4 has recently been implicated in early brain development and the genesis of the subcommissural organ (2). The functions of the remaining RFX factors are essentially unknown, although a few putative target genes have been reported, mainly for RFX1 (21, 33, 46, 47, 51). RFX1, RFX2, and RFX3 are the closest homologues of DAF-19 and dRFX. The *Rfx1*, *Rfx2*, and *Rfx3* genes are expressed at variable levels in a wide range of tissues (44). *Rfx3* is of particular interest because it is expressed preferentially in tissues containing ciliated cells, namely the brain, lungs, and testes (44).

In order to investigate the function of RFX3, we inactivated the *Rfx3* gene in mice. We show here that *Rfx3*-deficient mice have frequent LR asymmetry defects. This is due to the fact that there is an abnormal development of monocilia in the embryonic node. RFX3 is expressed specifically in the node and regulates at least one gene, *D2lic*, the homologues of which have been shown to be involved in IFT in other organisms. Our results thus demonstrate that the function of *Rfx* genes in cilium formation has indeed been conserved up to the level of mammals. However, our results also suggest that a specialization has arisen during the evolution of RFX regulatory cascades, since *Tg737*, a second gene implicated in IFT, does not appear to be controlled by RFX3.

MATERIALS AND METHODS

Generation of *Rfx3*-deficient mice. The conditional targeting vector for *Rfx3*-deficient mice contained two *loxP* sites inserted into the second and third introns flanking exon three of *Rfx3* and an *frt*-flanked neomycin resistance (*pgk-neo-pA*) cassette in the second intron (Fig. 1). The linearized targeting vector was transfected into ENS embryonic stem (ES) cells (13) by electroporation, and G418-resistant clones were selected as described previously (57). We screened for homologous recombination by a PCR using an internal primer and a primer situated downstream of the 3′ end of the targeting construct. Positive clones were confirmed by Southern blot analysis using 5′ and internal probes (Fig. 1). The *neoR* gene was excised with FLP recombinase from recombinant ES cell clones by transfection with the pCAGGS-Flpe vector (49) and selection with puromycin for 72 h. Clones were isolated and screened for G418 sensitivity. The correct excision of the *neoR* gene was controlled by Southern blot analysis with an internal probe. Correctly targeted ES cell clones containing ($Rfx3^{flox,neoR}$) or lacking ($Rfx3^{flox}$) the *neoR* gene were injected into C57BL/6J blastocysts and implanted into recipient females. Germ line transmission of the recombinant *Rfx3* allele was obtained for two chimeric mice generated with a $Rfx3^{flox,neoR}$ ES cell clone and for three chimeric mice generated with a $Rfx3^{flox}$ ES cell clone. For the generation of *Rfx3*-deficient mice, homozygous $Rfx3^{flox/flox}$ or $Rfx3^{flox,neoR/flox,neoR}$ mice were crossed with a deletion strain ubiquitously expressing Cre under the control of a cytomegalovirus promoter (50). The deletion of exon 3 was verified by Southern blotting. The resulting *Cre* +/$Rfx3^{flox}$ and *Cre* +/$Rfx3^{flox,neoR}$ progenies were backcrossed to C57BL/6J mice to eliminate the *Cre* transgene and then were bred to produce homozygous *Rfx3*-deficient mice. We confirmed by reverse transcription-PCR (RT-PCR) analysis and sequencing that no wild-type *Rfx3* mRNA was detected in the *Rfx3*-deficient embryos (data not shown). Mouse breeding and handling were carried out in a certified animal facility according to procedures that were approved by the local animal care and experimentation authorities.

Embryo staging and genotyping. Timed matings were set up between heterozygous *Rfx3*-deficient mice. The developmental stage of the embryos was estimated from the gestational time, with day 0.5 postcoitus being defined as the morning when a vaginal plug was detected. Pregnant mice were sacrificed by carbon dioxide asphyxiation, and placental and embryonic tissues were removed. The extra-embryonic tissues were frozen for subsequent genotyping and the embryos were rinsed with phosphate-buffered saline (PBS) prior to subsequent treatment. Genomic DNAs were prepared from ES cells, embryos, and mouse tails by proteinase K digestion, phenol-chloroform (24:1) extraction, and precip-

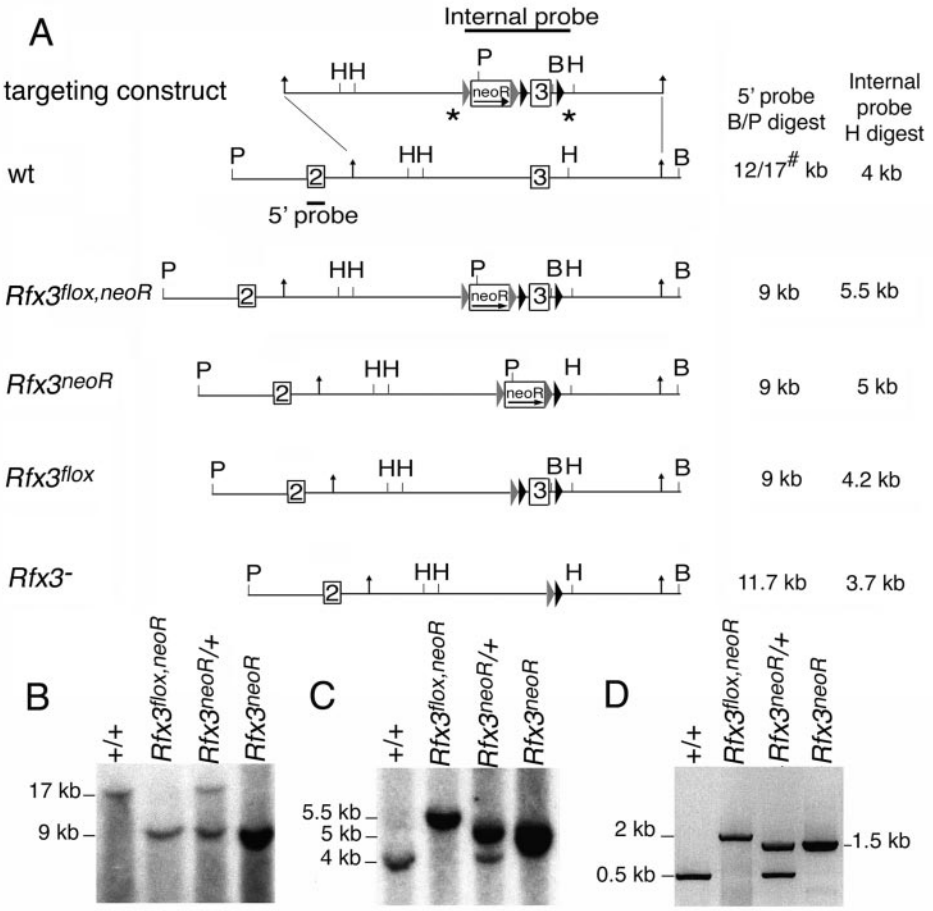

FIG. 1. Generation of *Rfx3*-deficient mice. (A) Schematic map of the mouse *Rfx3* gene, the targeting vector, and the different targeted alleles. FRT and Lox-P sites are represented by gray and black triangles, respectively. The orientation of the *neoR* gene is indicated by an arrow. HindIII (H), BamHI (B) and PstI (P) sites, the 5′ and internal probes used for Southern blot analysis, expected fragment sizes for the B-P and H digests, and PCR primers used for genotyping (*) are indicated. A restriction fragment length polymorphism (#) was observed for the B-P digests between the wild-type alleles from the 129 (12 kb) and C57BL/6 (17 kb) backgrounds. (B) Southern blot analysis of the $Rfx3^{flox,neoR}$ and $Rfx3^{neoR}$ alleles; B-P-digested genomic DNA was hybridized with the 5′ probe. Southern blot analysis of the $Rfx3^{-}$ and $Rfx3^{flox}$ alleles is not shown. (C) Southern blot analysis of the $Rfx3^{flox,neoR}$ and $Rfx3^{neoR}$ alleles; H-digested genomic DNA was hybridized with the internal probe. Southern blot analysis of the $Rfx3^{-}$ and $Rfx3^{flox}$ alleles is not shown. (D) Genotyping by PCR of genomic DNAs isolated from tail biopsies. The results show the amplification products obtained for mice carrying the wild-type (500 bp), $Rfx3^{flox,neoR}$ (2 kb), and $Rfx3^{neoR}$ (1.5 kb) alleles. Results for mice carrying the $Rfx3^{flox}$ (700 bp) and $Rfx3^{-}$ alleles (200 bp) are not shown.

itation with isopropyl alcohol. Genotyping was performed by PCR with primers M3.A (5′-GTC ATG CTG GAA AAT TTG AAG-3′) and M3.B (5′-AGT TGG CTT CTA ACT TCT ATG-3′).

Scanning electron microscopy. Genotyped embryos were fixed overnight at 4°C in 2% glutaraldehyde–0.1 M cacodylate buffer, pH 7.4. Embryos were washed several times in 0.2 M cacodylate buffer, pH 7.4, and were postfixed for 15 min in 1% OsO_4–0.1 M cacodylate buffer. The embryos were extensively washed with distilled water and dehydrated in a graded series of ethanol solutions, and lastly, in acetone. The embryos were then prepared for scanning electron microscopy by a critical point freeze-dry procedure (CPD020; Balzers-Union). The embryos obtained were surface coated by use of a gold-palladium spattering device (Hummer 2; Technics) under optimal conditions for 3 min 30 s and were observed with a scanning electron microscope (S800; Phillips) at 15 keV. Embryos were observed and photographed at identical magnifications. The ciliary lengths were measured for approximately 20 cilia per node.

Statistical analysis. The variations in ciliary length were analyzed by analysis of variance with two factors, the mutant or wild-type status and the embryonic stage (10 to 12). Analysis was done with the raw data as well as their natural logarithms, the former for absolute changes and the latter for relative changes. Assumptions of constant variance and normality were checked by using residual plots and quantile-quantile plots (58). Analysis was done with R software (20). The results of the analysis of variance with raw data as well as logarithm-transformed data showed strong evidence for the interaction mutant or wild type × stage ($P < 0.001$), that is, the differences between the mutant and wild-type ciliary lengths were dependent on the stage. For logarithm-transformed data, the differences between the mutant and the wild type increased from a nonsignificant difference for stage 10c ($P = 0.33$) to significant differences for all other stages ($P < 0.01$).

Whole-mount in situ hybridization. Single-stranded RNA probes containing digoxigenin were produced in vitro with T7 or T3 RNA polymerase (Roche Diagnostics) from an *Rfx3* cDNA clone (1,600 bp) inserted in pBluescript (Stratagene). The amount of RNA synthesized was determined by spotting aliquots of the probe onto a nylon filter along with digoxigenin-labeled standards (Roche Diagnostic), and detection was done with an antidigoxigenin antibody as described by the manufacturer (Roche Diagnostics). Whole-mount in situ hybridization was performed as described previously (8). *Rfx3* expression was examined after 2 h of incubation in Nitro Blue Tetrazolium-BCIP (5-bromo-4-chloro-3-indolylphosphate) (NBT/BCIP stock solution; Roche Diagnostics). Embryos were postfixed for 48 h at 4°C in 4% paraformaldehyde in TBS (137 mM NaCl, 25 mM Tris-HCl [pH 7.6], 3 mM KCl) and were photographed under a microscope. *nodal*, *lefta*, *leftb*, and *Hnf3 beta* expression was detected as previously described (60). The 1.4-kb *nodal* probe was obtained by BamHI restriction of a *nodal* cDNA. It recognizes *nodal* exon 3 and the 3′ end of exon 2.

TABLE 1. Analysis of frequency of homozygous *Rfx3*$^{neoR/neoR}$ embryos and incidence of LR asymmetry defects in two different mating schemes[a]

Cross or stage of development	Total no. of individuals	No. (%) of mutants	No. (%) of mutants with situs inversus	No. (%) of mutants with heterotaxy[b]
Rfx3$^{neoR/+}$ × *Rfx3*$^{neoR/+}$				
E8.5	151	31 (20)		
E10.5	88	31 (34)	5 (19)[c]	ND
E11–E12	67	9 (13)	ND	ND
E18	186	31 (17)	2 (6)	9 (29)
1 week PN	943	52 (6)	3 (6)	0
Rfx3$^{flox,neoR/flox,neoR}$ × *cre Rfx3*$^{neoR/+}$				
1 week PN	481	44 (9)	3 (7)	0

[a] ND, not determined; E, embryonic; PN, postnatal.
[b] Heterotaxy defects include all asymmetry defects other than situs inversus.
[c] Only 27 of 31 embryos were analyzed for embryo turning and cardiac looping inversion.

Whole-mount immunostaining. The anti-RFX3 rabbit antiserum used was described previously (41). The antibody was affinity purified with recombinant *Escherichia coli*-produced mouse RFX3. An anti-LIC3/D2LIC rabbit antiserum was obtained from A. Mikami (28). An anti-alpha-acetylated-tubulin mouse antibody was purchased from Sigma. Genotyped embryos were fixed for 1 h at room temperature in 4% paraformaldehyde in PBS, followed by permeabilization for 2 h at room temperature in PBST (PBS containing 0.1% Tween 20). Embryos were blocked for 2 h at room temperature with 2% bovine serum albumin in PBST. Incubation with the primary antibody (anti-RFX3 [1:100], anti-D2LIC, or anti-acetylated-tubulin [1:150]) was performed overnight at 4°C. After being thoroughly washed with PBST, embryos were incubated overnight at 4°C with a Cy3-conjugated goat anti-rabbit or -mouse antibody or an Alexa 488-conjugated goat anti-rabbit antibody (Molecular Probes; 1:500). Embryos were washed extensively in PBST, mounted in 50% glycerol in PBS, and observed with a Zeiss confocal microscope (LSM 510).

Histology. Organs were fixed for 1 week at 4°C in Boin fixative and then dehydrated with a graded series of butanol. The samples were embedded in paraffin, cut onto slides (Superfrost; CML), and stained with hematoxylin and eosin.

Quantitative RT-PCR. Total RNAs were extracted from precisely staged E7.5 embryos by use of TRIzol reagent (Invitrogen). RT was performed with RNAs derived from single embryos with primers specific for each gene and with Superscript II reverse transcriptase (Life Technologies). Real-time PCR analysis was performed by SYBR Green fluorescent PCR (Qiagen) in a LightCycler fluorescence temperature cycler (Roche Molecular Biochemicals, Mannheim, Germany) according to the manufacturer's instructions. The primers used were as follows: for D2LIC, 5′-AGA CCC GCA GTA TGC AGA AA-3′ and 5′-GAG TCC AGC TCG ATT TGC TT-3′ or 5′-GAG ATG CGG CAA CGA ATG TG-3′ and 5′-AGC GAG GCT CCG TAG TAA TG-3′; for TG737, 5′-CCG AAT GGC CTT AGA TCA GA-3′ and 5′-CAT GCT CAT GAT GTG CTC AA-3′; for glyceraldehyde-3-phosphate dehydrogenase, 5′-GTG TTC CTA CCC CCA ATG TG-3′ and 5′-AGG AGA CAA CCT GGT CCT CA-3′; and for TATA binding protein (TBP), 5′-ATG CTG AAT ATA ATC CCA AGC GA-3′ and 5′-GAA AAT CAA CGC AGT TGT CCG-3′. Primers were used at a concentration of 10 μM. The PCR conditions were as follows: 95°C for 15 min; 5 cycles of 95°C for 15 s, 62°C for 20 s, and 72°C for 30 s; 20 cycles of 95°C for 15 s, 62 to 52°C (−0.5°C/cycle) for 20 s, and 72°C for 30 s; and 20 cycles of 95°C for 15 s, 52°C for 20 s, and 72°C for 30 s. According to a melting point analysis, only one PCR product was amplified under these conditions. RNAs extracted from wild-type embryos were used to generate a standard curve for each gene. Results were normalized with respect to the internal controls and are expressed relative to the levels found in wild-type embryos at the same stage.

RESULTS

Generation of *Rfx3*-deficient mice. We used homologous recombination in ES cells to generate two different "floxed" alleles of *Rfx3* (Fig. 1). In each allele, the exon encoding the DNA binding domain (exon 3) is flanked by Lox-P sequences. In one allele (*Rfx3*^{flox,neoR}), the neomycin resistance (*neoR*) gene was retained within the intron situated upstream of exon 3. In the second allele (*Rfx3*^{flox}), the *neoR* gene was removed by FLP-mediated excision in ES cells. Mice that were homozygous for the *Rfx3*^{flox,neoR} or *Rfx3*^{flox} allele exhibited normal viability and fertility, and no particular phenotype was observed. *Rfx3* knockout mice were then generated by two approaches. First, stable mouse strains carrying a deletion of exon 3 (*Rfx3*^{neoR} and *Rfx3*$^{-}$ alleles) were produced by crossing the floxed mice (*Rfx3*^{flox,neoR} and *Rfx3*^{flox} alleles) with a mouse strain carrying a *Cre* deletion transgene. As an alternative approach, *Rfx3*-deficient offspring were also obtained directly from crosses between *Cre Rfx3*$^{+/-}$ and *Rfx3*$^{flox/flox}$ mice. In the latter case, a PCR strategy was used to show that <1% of the nondeleted allele was retained in the *Rfx3*-deficient offspring (data not shown).

Exon 3 is essential because it encodes the DNA binding domain. Moreover, RT-PCR experiments have shown that the deletion of exon 3 results in the splicing of exon 2 to exon 4, which leads to a frameshift and premature termination at an out-of-frame stop codon (data not shown). The deletion of exon 3 thus constitutes a strong loss-of-function mutation.

All studies were performed in parallel with mice carrying the *Rfx3*^{neoR} and *Rfx3*$^{-}$ alleles. No significant differences were observed between these two strains, indicating that retention of the *neoR* gene has no effect on the phenotype. For the sake of simplicity, only the results obtained with mice carrying the *Rfx3*^{neoR} allele are presented.

***Rfx3*-deficient mice exhibit a high rate of embryonic lethality.** Instead of the 25% expected from normal Mendelian inheritance, only 6% of the pups born from *Rfx3*$^{+/neoR}$ intercrosses are homozygous *Rfx3*$^{neoR/neoR}$ mutants. The majority of *Rfx3*-deficient mice thus die during embryogenesis. Embryos were genotyped at different developmental stages to establish when lethality occurs (Table 1). Two peaks of death were observed. Approximately half of the homozygous *Rfx3*$^{neoR/neoR}$ embryos died around days 11 or 12 of embryonic development. Of the embryos that survived past this stage, approximately two-thirds died at birth.

Rfx3-deficient mice are systematically smaller (Fig. 2). Their body weights at birth are approximately one-third lower than those of wild-type or heterozygous littermates. This growth retardation increases with age, and the body weights that adult *Rfx3*-deficient male or female mice attain are less than half those of their control sibs. There is also a modest growth

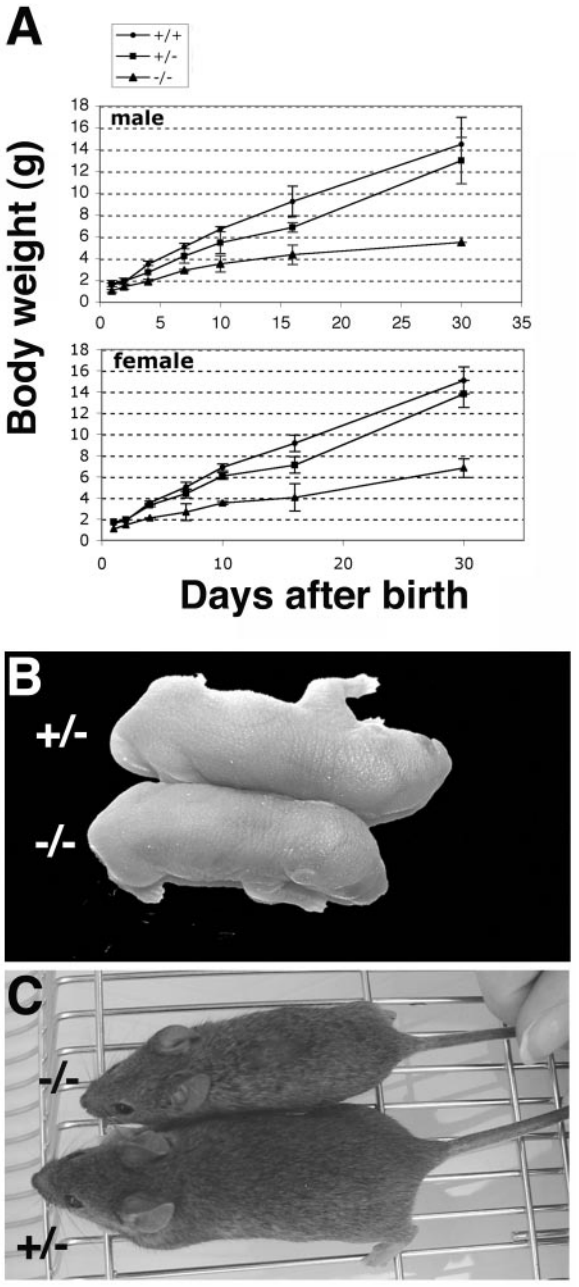

FIG. 2. *Rfx3*-deficient mice exhibit growth retardation. (A) Body weights of homozygous *Rfx3*-deficient ($Rfx3^{-/-}$) and control ($Rfx3^{+/-}$ and $Rfx3^{+/+}$) littermates compared for males or females at different ages, ranging from newborn pups to adults. At least five individuals of each genotype were weighed at each stage except for the point for mutant males at day 30, for which only one male remained alive. Representative *Rfx3* deficient (−/−) and control (+/−) newborn pups (B) and adults (C) are shown to illustrate the differences in size.

retardation in heterozygous mice, suggesting that there may be a certain degree of haploinsufficiency for certain functions of RFX3.

LR asymmetry defects in *Rfx3*-deficient mice. Remarkably, approximately 6% of newborn *Rfx3*-deficient pups had situs inversus, that is, they had a complete inversion of the LR distribution of the visceral organs (Table 1; Fig. 3). No other types of laterality defects were observed after birth. To document further the defect in LR determination, we examined 18-day-old embryos for the positions of several organs (Table 2). Thirty-five percent of the *Rfx3*-deficient embryos had asymmetry defects. Of these, 6% had situs inversus and 29% had incomplete inversion defects (heterotaxy). The majority of embryos with heterotaxy defects showed left pulmonary isomerism (9 of 10) or meso- or dextrocardia (6 of 10) (Table 2; Fig. 3). The dextro- and mesocardia phenotypes were associated with cardiac malformations (data not shown). Fewer embryos were observed with asymmetry defects of the stomach, liver, and kidney (Table 2). Since only situs inversus was observed in newborn pups, it is likely that the heterotaxy defects accounted for the strong lethality observed at birth. We cannot exclude that other causes of organ failure might have also contributed to the high lethality rate at birth. However, we did not observe any major visceral organ malformations other than laterality defects. We also observed an inversion of embryo turning and cardiac looping in 19% of the mutant embryos at day 10.5 (Table 1; Fig. 3). Defects in the determination of the LR body axis could thus also explain the peak of lethality observed between days 10.5 and 12.5 of embryonic development.

nodal is currently the earliest gene known to be asymmetrically expressed in the mouse embryo. This asymmetry is first detected as an enhanced expression of the gene in the cells bordering the left side of the node at the early-head-fold stage (7, 24). This limited domain of asymmetric *nodal* expression is then expanded to the left lateral plate mesoderm, where *leftb* is also expressed (for a review, see reference 16). *lefta* is expressed in the left side of the prospective neural floor plate, where it may function as part of the midline barrier. Given the frequent LR asymmetry defects observed in the *Rfx3*-deficient mice, we examined *nodal* and *lefta*/*b* expression in the mutant embryos. We observed an abnormal bilateral expression of *nodal* and *lefty* in some *Rfx3*-deficient embryos (three of five embryos) (Fig. 3K and L). However, *nodal* and *lefty* expression was not fully symmetrical, as it was weaker on the right side. Organ isomerization in *Rfx3* mutants was not complete and affected mainly the anterior organs, such as the lungs. The partial bilateral symmetry of *nodal* and *lefta*/*b* expression could be relevant to this preferential anterior isomerization. We did not observe a defect in *HNF3beta* expression in the midline ($n = 10$ embryos [data not shown]), suggesting that the deficiency in RFX3 does not severely affect this structure.

Taken together, the results indicate that a deficiency in RFX3 results in a severe perturbation of the mechanisms controlling LR asymmetry determination during embryonic development. In contrast to what was observed for growth retardation, no laterality defects have been observed in heterozygous mice, indicating that there is no obvious haploinsufficiency in this system.

***Rfx3* directs the development of nodal monocilia.** The development of LR asymmetry is controlled in part by cellular mechanisms taking place in the embryonic node. We therefore determined whether *Rfx3* is expressed in this structure. We found that RFX3 mRNA (Fig. 4A) and protein (Fig. 4B) are indeed detected specifically in the node at 7.5 days of development.

Since RFX factors are involved in cilium formation in *C. elegans* and *D. melanogaster*, we examined by scanning electron

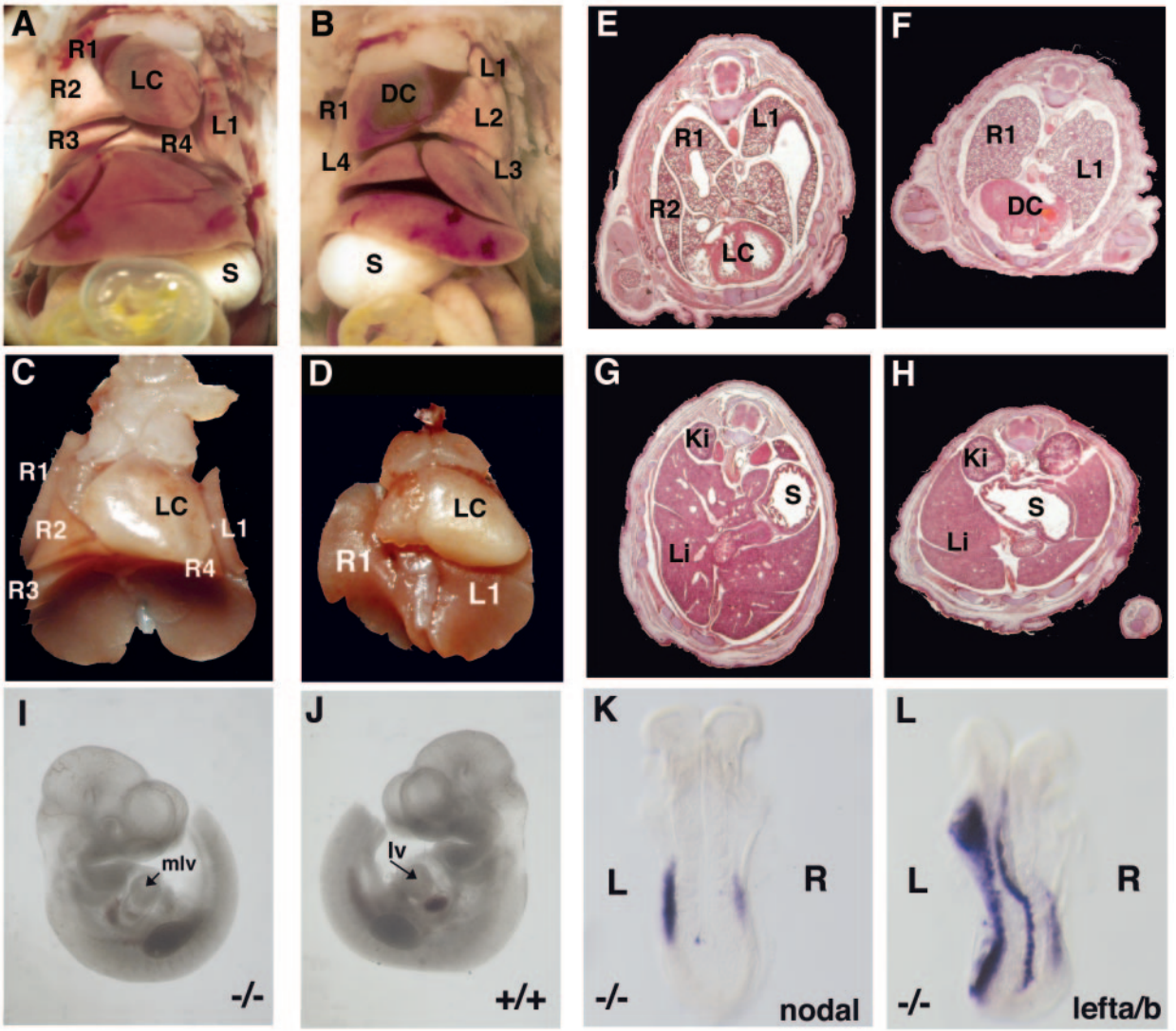

FIG. 3. *Rfx3*-deficient mice show characteristic LR asymmetry defects. (A and B) Dissections of 3-week-old control (A) and *Rfx3*-deficient (B) mice. The mutant mouse had a completely reversed orientation of the visceral organs (situs inversus). (C and D) Dissections of 18-day-old control (C) and *Rfx3*-deficient (D) embryos. The mutant mouse had a left pulmonary isomerism. (E to H) Transverse histological sections of 18-day-old control (E and G) and *Rfx3*-deficient (F and H) embryos showing various asymmetry defects, including left pulmonary isomerism, dextrocardia, and a central stomach. (I and J) Orientation of cardiac looping and embryo turning in 10.5-day-old control (left side view) (J) and mutant (right side view) (I) embryos. The mutant embryo had an inversion of cardiac looping and embryonic turning. The tail bud was removed to improve visualization of the heart. (K and L) In situ hybridization of *Rfx3* knockout embryos with nodal and lefty probes. The latter probe detects both *lefta* and *leftb* expression, in the prospective floor plate and lateral plate mesoderm, respectively. Abnormal bilateral expression of *nodal* and *lefta/b* was observed in the *Rfx3*-deficient embryos (dorsal view). R1 to -4, right pulmonary lobes 1 to 4; L1 to -4, left pulmonary lobes 1 to 4; DC, dextrocardia; LC, levocardia; S, stomach; Li, liver; Ki, kidney; L, left; R, right; lv, left ventricle; mlv, morphological left ventricle.

microscopy whether the deficiency in *Rfx3* affects the development of cilia in the embryonic node. Cilia were present in the nodes of all *Rfx3*-deficient embryos examined ($n = 16$). However, a careful analysis of precisely timed embryos ranging from 7.25 to 8 days indicated that the growth of nodal cilia was significantly delayed in the mutant embryos with respect to wild-type embryos (Fig. 4C). At early stages, such as the late-streak nodal stage (staging according to reference 56), cilia in the mutant and wild-type embryos were similar in number and had the same relatively short lengths (average, 1.5 μm) (Fig. 4D to G). At later stages, however, significant differences in the lengths of the nodal monocilia were observed between the mutant and wild-type embryos. As development proceeded, the lengths of the cilia increased considerably in wild-type embryos, but not in the *Rfx3*-deficient mutants (Fig. 4H to K). By the early-head-fold stage, the cilia in wild-type embryos were twice as long (average, 3 μm) as those in the *Rfx3* mutants (average, 1.5 μm) (Fig. 4L to O). The growth of cilia in the mutant embryos was thus strongly perturbed.

***Rfx3* regulates a dynein gene.** To understand how *Rfx3* affects the growth of cilia in the embryonic node, we examined the expression of mouse homologues of *C. elegans* genes that are known to be regulated by DAF-19 and implicated in sensory cilium differentiation in this organism. We first concen-

TABLE 2. Heterotaxy defects observed in 18.5-day-old mutant embryos

Embryo no.	Heart condition	Lung lobation	Stomach position[b]	Relative kidney position	Spleen position	Liver lobation
1	Mesocardia	Left isomerism	Central	Symmetric	N	ND
2	Dextrocardia	2LL/3RL	Right	Inverted	ND	ND
3	Levocardia	Left isomerism	N	N	ND	ND
4	Levocardia	Left isomerism	N	N	ND	ND
5	Mesocardia	Left isomerism	N	N	N	N
6	Dextrocardia	Left isomerism	Right	Inverted	Inverted	Inverted
7	Dextrocardia	Left isomerism	N	N	N	N
8	Levocardia	Left isomerism	N	N	N	N
9	Atrophy	Left isomerism	N	Same level	ND	Symmetric
10[a]	Mesocardia	Left isomerism	Central	Same level	ND	ND

[a] This embryo was not included in Table 1 because its littermates were lost during typing.
[b] N, normal position of organs; ND, not determined; 2LL/3RL, two left lobes and three right lobes.

trated on *polaris*/*Tg737*, the mouse homologue of the *osm-5* gene of *C. elegans*. *Tg737* appeared to be a likely target of RFX3 because mice with null mutations in this gene lack cilia in the embryonic node and exhibit defects in LR asymmetry (29). Moreover, there are putative RFX binding sites in the upstream region of the *Tg737* gene (data not shown). We therefore compared *Tg737* mRNA expression in mutant and wild-type embryos at 7.5 days of development by quantitative RT-PCR (Fig. 5A). Surprisingly, no significant difference in *Tg737* expression was observed. We also did not detect an effect of the *Rfx3* mutation on *Tg737* mRNA expression in adult tissues (kidneys, brains, lungs, and testes) containing ciliated cells (data not shown). Taken together, these results suggest that *Tg737* is in fact not a target of RFX3. This is consistent with the fact that, in contrast to what is found in *Tg737*-deficient mice, no obvious kidney defects were observed in the *Rfx3* knockout mice. It is also consistent with the finding that RFX3 is not expressed at a high level in the kidney (data not shown).

We next examined *D2lic*, the mouse homologue of *xbx-1*, a more recently identified target gene of DAF-19 in *C. elegans* (48). The *xbx-1* gene, as well as its homologue *DLIC* in *Chlamydomonas*, is involved in retrograde IFT. In mammals, D2LIC was first identified as a cofactor of the cytoplasmic dynein DHC2 (14). It is expressed in various ciliated cell types, such as primary ciliated kidney cells (MDCK cells and ciliated efferent duct cells), ciliated lung epithelial cells, and ciliated cells of the ventricles in the brain (28, 40). In these cells, D2LIC colocalizes at sites of axonemal assembly with other proteins involved in cilium formation, such as Polaris and β-tubulin (40). Consistent with a role in the development of nodal cilia, D2LIC expression can be detected in the node by immunostaining (Fig. 5C). An analysis of *D2lic* expression by quantitative RT-PCR revealed that D2LIC mRNA levels were significantly reduced in *Rfx3*-deficient embryos at 7.5 days of development. Thus, in contrast to *Tg737*, *D2lic* expression is indeed under the control of RFX3. D2LIC mRNA expression was reduced only 40%. The fact that the reduction was only partial is consistent with the fact that the D2LIC protein remained detectable in the nodes of mutant embryos (Fig. 5C), although this expression was slightly reduced in intensity and appeared more diffuse.

To strengthen the finding that RFX3 is involved in the expression of the *D2lic* gene, we examined the levels of *D2lic* mRNA in various embryonic and adult tissues containing ciliated cells (brains, lungs, kidneys, and testes). A variable reduction in *D2lic* mRNA expression was consistently observed. This was particularly evident for the adult brain, in which a reduction ranging from two- to over fivefold (average, threefold) was observed (Fig. 5B). Similar 2- to 10-fold reductions were observed in lungs, kidneys, and testes (data not shown).

DISCUSSION

We show here that *Rfx3*-deficient mice exhibit frequent defects in the specification of the asymmetric LR body axis. This is due to the fact that RFX3 is expressed in ciliated cells of the embryonic node, where it controls the expression of genes required for normal growth of the nodal monocilia. One of the target genes regulated by RFX3 is *D2lic*, a gene functioning in the IFT process required for the assembly and maintenance of cilia. Together with the recent findings that DAF-19 and dRFX control the formation of sensory cilia in *C. elegans* and *D. melanogaster* and that DAF-19 regulates the *C. elegans* homologue of *D2lic*, our results demonstrate that members of the RFX family of transcription factors have retained a highly conserved and pivotal regulatory role in ciliogenesis in a wide range of species.

In addition to the defects in the establishment of the LR body axis, *Rfx3*-deficient mice exhibited marked growth retardation. The reason for the retarded growth phenotype is not known. It may be relevant that *Rfx1* has recently been implicated in the regulation of growth hormone gene expression in the pituitary gland (33). *Rfx3* could perhaps also play a role in the regulation of growth hormone expression. In this respect, it is interesting that *Rfx3* is indeed expressed in the pituitary gland (unpublished results). However, numerous other defects could also result in growth retardation and this question will therefore require further investigation.

Less than half of the *Rfx3*-deficient mice showed heterotaxy. This is somewhat less frequent than what is observed for other mouse models exhibiting LR asymmetry abnormalities resulting from defects in nodal cilia. This may be a consequence of the fact that cilia remain present in the nodes of *Rfx3*-deficient embryos. Although stunted, these cilia may be able to produce a nodal flow that is sufficient to install a correct pattern of LR asymmetry in part of the embryos. This suggests that there may be a general correlation between the incidence of asymmetry

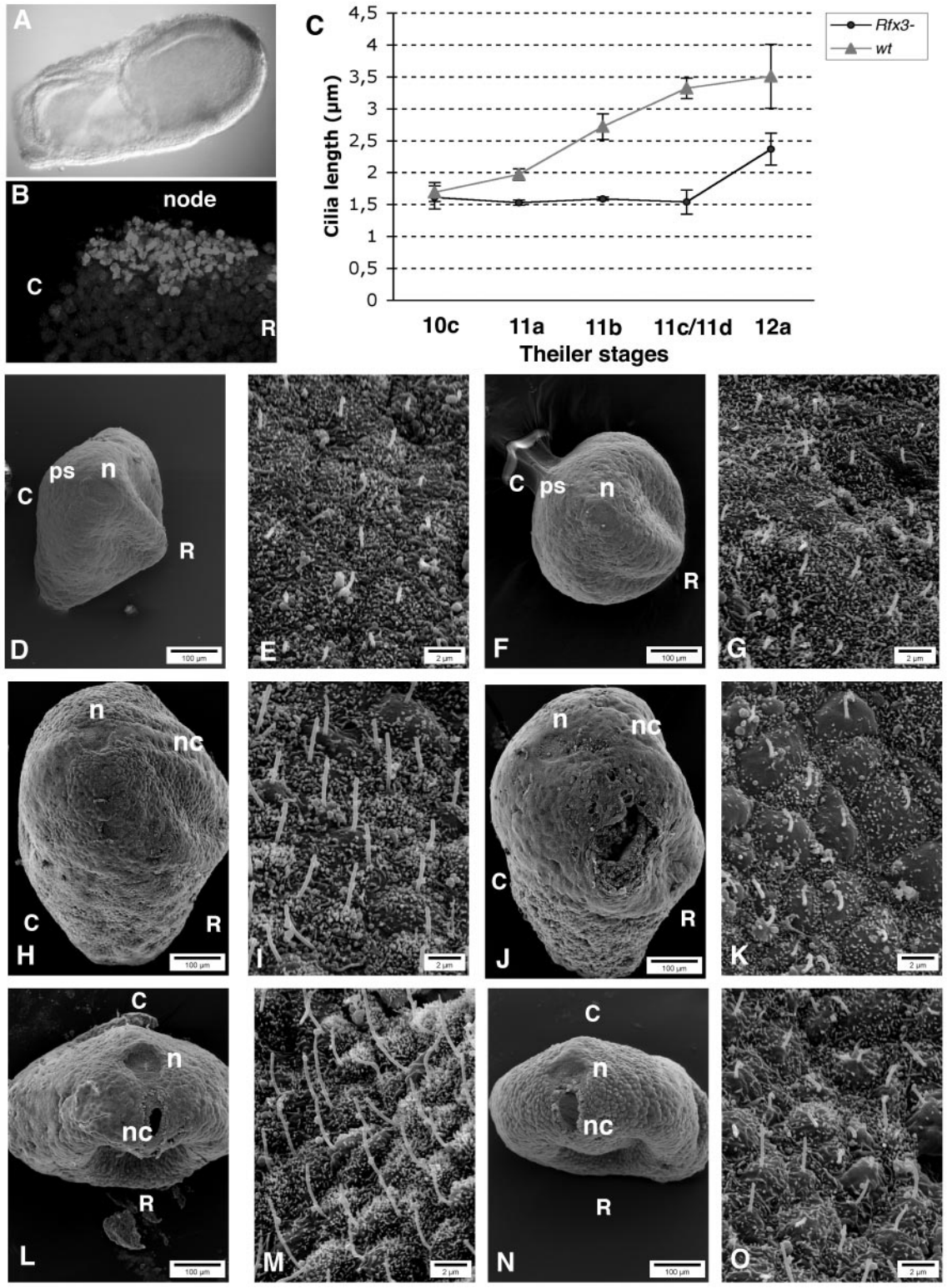

FIG. 4. *Rfx3* is expressed in the embryonic node and regulates ciliary growth. The localization of Rfx3 mRNA (A) and protein (B) was examined in the embryonic node at E7.5. (C) Changes in the lengths of node monocilia between 7 and 8 days of embryonic development in control and mutant embryos. Theiler stage 10c, late streak, early bud; Theiler stage 11a, early neural plate; Theiler stage 11b, late neural plate; Theiler stage 11c/11d, early to late head fold; Theiler stage 12a, one to three somites. (D to O) Scanning electron micrographs of the embryonic nodes of wild-type (D, E, H, I, L, and M) and *Rfx3*-deficient (F, G, J, K, N, and O) embryos at three different stages. For each embryo, two magnifications are presented to show the position of the node and the nodal monociliated cells. At late streak stages (D to G), the node monocilia were of similar sizes (average, 1.6 μm) in control (D and E [$n = 6$]) and *Rfx3*-deficient (F and G [$n = 4$]) embryos. By the late neural plate stage (H to K), the

errors and the severity of the ciliary defects. Although no studies have addressed this question directly, a number of observations are consistent with this correlation. For example, in mice carrying *Tg737* null alleles the nodal monocilia are completely absent and a high frequency of heterotaxy defects is observed, while no heterotaxy phenotype is observed in mice carrying the hypomorphic *Tg737*^{orpk} allele. However, it should also be mentioned that the severity of the abnormal asymmetry phenotype cannot always be correlated with the apparent gravity of the ciliary defects. For instance, although all mutant *inv* mice have a reversal of the LR body pattern, the nodal cilia are present normally and show only a modest reduction in motility. The latter example suggests that the flow efficiency driven by nodal cilia is not the only determinant of nodal control over LR asymmetry. To our knowledge, this is the first report describing an increase in the length of cilia in the embryonic node between days E7.25 and E8 of normal mouse development. However, it has been shown previously that nodal flow evolves during nodal development (34). Soon after nodal formation, the cilia are immotile. They then start to move, and by the mid-neural-plate stage the rotating cilia produce local vortices. Movement subsequently becomes coordinated further such that by the late-neural-plate stage a smooth leftward flow is produced. Variations in cilium length during nodal development could well underlie this evolution of the nodal flow. The delay in growth of the cilia in the nodes of *Rfx3*-deficient embryos could thus result in LR patterning defects because it is responsible for an altered or temporally perturbed nodal flow. We cannot rule out that other defects within the nodal cilia could also contribute to an altered mobility and a nodal flow defect. However, no gross ultrastructural defects have been observed in mutant nodal cilia by transmission electron microscopy (data not shown). Nodal flow measurements in *Rfx3* mutant embryos, correlated with a fine temporal analysis of the first asymmetric gene expression patterns, will be of particular interest for understanding the relationships between ciliary growth, nodal flow, and LR asymmetry breakage.

We have identified *D2lic* as one of the target genes regulated by RFX3 in the embryonic node and in adult tissues. *D2lic* expression was reduced only partially in the *Rfx3*-deficient embryos. This is consistent with the finding that cilia remain present in the mutant nodes, although they fail to grow to their normal length. We suspect that a complete inactivation of *D2lic* would result in a total loss of node monocilia, as is observed, for example, for null alleles of *Tg737*.

So far, all genes shown to be regulated by DAF-19 in *C. elegans* are involved in B complex assembly or the retrograde transport of IFT particles (18, 41, 48). These DAF-19 target genes include the *C. elegans* homologues of both *D2lic* (*xbx-1*) and *Tg737* (*osm-5*). It was consequently rather surprising that the expression of *D2lic*, but not of *Tg737*, was affected in *Rfx3*-deficient mice (Fig. 5). These results imply that RFX3

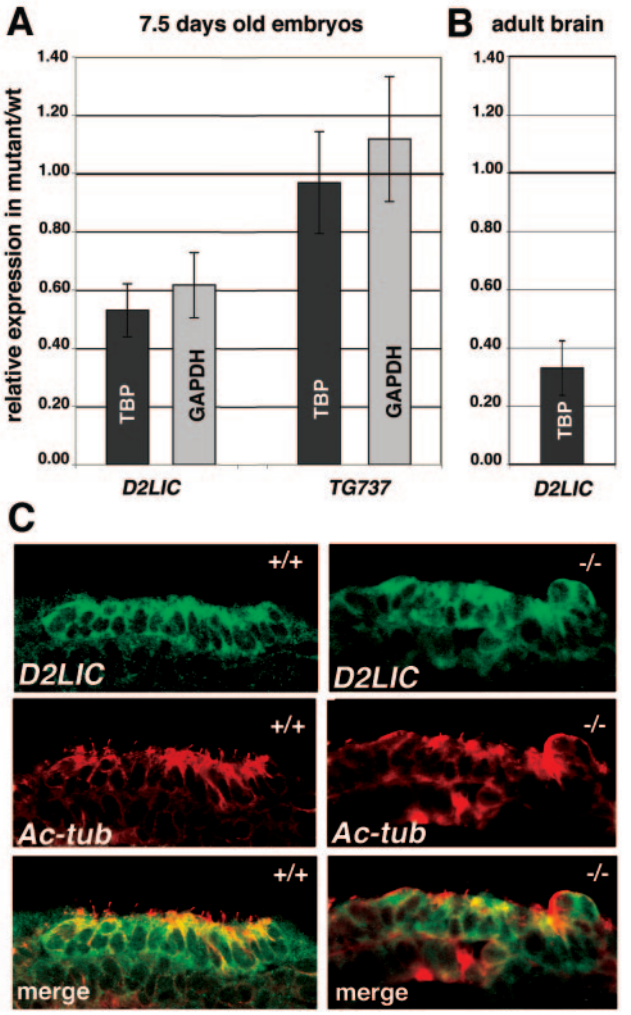

FIG. 5. *Rfx3* regulates *D2liC* expression in ciliated node cells and the adult brain. (A) *D2liC* and *Tg737* mRNA expression was quantified by real-time RT-PCR for wild-type and *Rfx3*-deficient embryos at E7.5. Quantification was normalized with respect to two different control mRNAs, TBP and glyceraldehyde-3-phosphate dehydrogenase. The results are presented as the expression levels in mutant versus wild-type embryos. *D2liC* expression was significantly reduced in *Rfx3*-deficient embryos. *Tg737* expression did not differ significantly between the wild-type and *Rfx3*-deficient embryos. The means and standard deviations from experiments performed with three to five independent embryos of each genotype are shown. (B) *D2liC* mRNA expression was quantified by real-time RT-PCR in brain RNAs prepared from wild-type and *Rfx3*-deficient adults. Quantification was normalized with respect to TBP mRNA. The results are presented as the expression levels in mutant versus wild-type embryos. The means and standard deviations from three experiments are shown. (C) D2LIC protein is expressed (green) in the monociliated embryonic node cells in wild-type and mutant embryos. Cilia are labeled (red) with antibodies against acetylated tubulin. Bottom panels, merge of D2LIC and acetylated tubulin staining.

cilia were longer in control embryos (average, 2.7 μm; $n = 3$) (H and I) but had not grown in *Rfx3*-deficient embryos (average size, 1.6 μm; $n = 3$) (J and K). This difference was even greater at stage 11c/11d, when cilia in control embryos had an average size of 3.3 μm (L and M [$n = 3$]), whereas cilia in the *Rfx3*-deficient embryos still had an average length of only 1.5 μm (N and O [$n = 2$]). The apparent morphological alteration of the mutant node in panel N is not significant as it was not observed for all mutant embryos. At late somite stages, the nodal monocilia in the mutants started to grow slightly but remained half as long as in the controls (data not shown). Bars, 100 μm (D, F, H, J, L, and N) and 2 μm (E, G, I, K, M, and O). n, node; nc, notochord; ps, primitive streak; R, rostral; C, caudal.

governs the expression of only a subset of the proteins required for IFT particle transport and B complex assembly in the mouse, indicating that additional key regulators must regulate the expression of the other components. One interesting candidate is the HFH-4 transcription factor. Mice lacking HFH-4 have a phenotype that is very similar to that of our RFX3-deficient mice (3). So far, the expression of only one gene, *Lrd*, has been shown to be reduced in HFH-4-deficient mice (3). It is therefore possible that RFX factors and HFH-4 collaborate by controlling complementary or overlapping sets of target genes. The RFX1 and RFX2 transcription factors are also prime candidates because they exhibit strong homology to RFX3 and recognize the same binding sites (44). It is tempting to speculate that the different mammalian RFX factors have become specialized for the activation of distinct subsets of IFT genes. Alternatively, it is also possible that the three RFX factors regulate overlapping sets of genes, perhaps displaying a functional redundancy at certain genes but not at others. This second possibility could explain why the loss of RFX3 has only a partial effect on *D2lic* expression. Both models could also account for the fact that a deficiency in RFX3 does not affect *Tg737* expression in either the embryonic node or adult tissues, despite the fact that this gene does contain typical RFX binding sites in its upstream region. Genetic inactivation of the *Rfx1* and *Rfx2* genes will allow us to define the eventual redundant or specific roles of the different RFX transcription factors in cilium formation and function.

The molecular mechanisms involved in cilium assembly and maintenance appear to be largely the same for many different types of cilia and flagella. For example, mutations in *Tg737* and *Hfh-4* affect both the cilia found in the node and those found in other tissues and cell types. We anticipate that the inactivation of *Rfx3* could have similar consequences. The analysis of several different types of ciliated cells in our knockout mice will allow us to determine if *Rfx3* plays a role in the development of all or many types of cilia or whether it is only important for primary nodal cilia.

Several human diseases result from ciliary defects (for reviews, see references 37 and 52). Among these diseases, primary ciliary dyskinesia (PCD) is an autosomal recessive syndrome characterized by immotile cilia, recurrent respiratory tract infections leading to bronchiectasis, male sterility, and most notably situs inversus in half of the patients (Kartagener syndrome). So far, most of the genes affected in PCD have not been identified. The phenotype of *Rfx3*-deficient mice suggests that mutations in the human *RFX3* gene could account for certain PCD cases. Genes regulated by RFX3, such as *D2LIC*, are also potential candidates implicated in human cilium-related disorders. Dissection of the RFX3 regulatory cascades in mice could thus contribute to the identification of molecular defects underlying human cilium-related disorders.

ACKNOWLEDGMENTS

Work in the laboratory of B. Durand was supported by the CNRS, the ACI Bio du Developpement et Physiologie Intégrative and the Région Rhône Alpes Program. Work in the laboratory of W. Reith was supported by the Swiss National Science Foundation (grant 3100-064895). D. Baas was supported by a fellowship from the Région Rhône Alpes. E. Bonnafe was supported by a doctoral fellowship from the French Research Ministry. M. Touka was supported by a doctoral fellowship from the Egide Foundation.

We thank Nigel Yoccoz for the efficient statistical analysis of the data and Denise Aubert for valuable help with ES cell technology and ES cell transfer. We are grateful to Peter Swoboda for valuable discussions and for the communication of results and information prior to publication. We thank A. Mikami and R. Vallee for the generous gift of D2LIC antibodies. We thank H. Hamada for the generous gift of the plasmids for generating *lefty* probes.

REFERENCES

1. **Bartoloni, L., J. L. Blouin, Y. Pan, C. Gehrig, A. K. Maiti, N. Scamuffa, C. Rossier, M. Jorissen, M. Armengot, M. Meeks, H. M. Mitchison, E. M. Chung, C. D. Delozier-Blanchet, W. J. Craigen, and S. E. Antonarakis.** 2002. Mutations in the DNAH11 (axonemal heavy chain dynein type 11) gene cause one form of situs inversus totalis and most likely primary ciliary dyskinesia. Proc. Natl. Acad. Sci. USA **99:**10282–10286.
2. **Blackshear, P. J., J. P. Graves, D. J. Stumpo, I. Cobos, J. L. Rubenstein, and D. C. Zeldin.** 2003. Graded phenotypic response to partial and complete deficiency of a brain-specific transcript variant of the winged helix transcription factor RFX4. Development **130:**4539–4552.
3. **Brody, S. L., X. H. Yan, M. K. Wuerffel, S. K. Song, and S. D. Shapiro.** 2000. Ciliogenesis and left-right axis defects in forkhead factor HFH-4-null mice. Am. J. Respir. Cell. Mol. Biol. **23:**45–51.
4. **Brueckner, M.** 2001. Cilia propel the embryo in the right direction. Am. J. Med. Genet. **101:**339–344.
5. **Chen, J., H. J. Knowles, J. L. Hebert, and B. P. Hackett.** 1998. Mutation of the mouse hepatocyte nuclear factor/forkhead homologue 4 gene results in an absence of cilia and random left-right asymmetry. J. Clin. Investig. **102:** 1077–1082.
6. **Cole, D. G., D. R. Diener, A. L. Himelblau, P. L. Beech, J. C. Fuster, and J. L. Rosenbaum.** 1998. Chlamydomonas kinesin-II-dependent intraflagellar transport (IFT): IFT particles contain proteins required for ciliary assembly in Caenorhabditis elegans sensory neurons. J. Cell Biol. **141:**993–1008.
7. **Collignon, J., I. Varlet, and E. J. Robertson.** 1996. Relationship between asymmetric nodal expression and the direction of embryonic turning. Nature **381:**155–158.
8. **Conlon, R. A., and J. Rossant.** 1992. Exogenous retinoic acid rapidly induces anterior ectopic expression of murine Hox-2 genes in vivo. Development **116:**357–368.
9. **Dubruille, R., A. Laurencon, C. Vandaele, E. Shishido, M. Coulon-Bublex, P. Swoboda, P. Couble, M. Kernan, and B. Durand.** 2002. Drosophila regulatory factor X is necessary for ciliated sensory neuron differentiation. Development **129:**5487–5498.
10. **Emery, P., B. Durand, B. Mach, and W. Reith.** 1996. RFX proteins, a novel family of DNA binding proteins conserved in the eukaryotic kingdom. Nucleic Acids Res. **24:**803–807.
11. **Essner, J. J., K. J. Vogan, M. K. Wagner, C. J. Tabin, H. J. Yost, and M. Brueckner.** 2002. Conserved function for embryonic nodal cilia. Nature **418:** 37–38.
12. **Gajiwala, K. S., H. Chen, F. Cornille, B. P. Roques, W. Reith, B. Mach, and S. K. Burley.** 2000. Structure of the winged-helix protein hRFX1 reveals a new mode of DNA binding. Nature **403:**916–921.
13. **Gauthier, K., O. Chassande, M. Plateroti, J. P. Roux, C. Legrand, B. Pain, B. Rousset, R. Weiss, J. Trouillas, and J. Samarut.** 1999. Different functions for the thyroid hormone receptors TRalpha and TRbeta in the control of thyroid hormone production and post-natal development. EMBO J. **18:**623–631.
14. **Grissom, P. M., E. A. Vaisberg, and J. R. McIntosh.** 2002. Identification of a novel light intermediate chain (D2LIC) for mammalian cytoplasmic dynein 2. Mol. Biol. Cell **13:**817–829.
15. **Guichard, C., M. C. Harricane, J. J. Lafitte, P. Godard, M. Zaegel, V. Tack, G. Lalau, and P. Bouvagnet.** 2001. Axonemal dynein intermediate-chain gene (DNAI1) mutations result in situs inversus and primary ciliary dyskinesia (Kartagener syndrome). Am. J. Hum. Genet. **68:**1030–1035.
16. **Hamada, H., C. Meno, D. Watanabe, and Y. Saijoh.** 2002. Establishment of vertebrate left-right asymmetry. Nat. Rev. Genet. **3:**103–113.
17. **Haycraft, C. J., J. C. Schafer, Q. Zhang, P. D. Taulman, and B. K. Yoder.** 2003. Identification of CHE-13, a novel intraflagellar transport protein required for cilia formation. Exp. Cell Res. **284:**249–261.
18. **Haycraft, C. J., P. Swoboda, P. D. Taulman, J. H. Thomas, and B. K. Yoder.** 2001. The C. elegans homolog of the murine cystic kidney disease gene Tg737 functions in a ciliogenic pathway and is disrupted in osm-5 mutant worms. Development **128:**1493–1505.
19. **Ibanez-Tallon, I., S. Gorokhova, and N. Heintz.** 2002. Loss of function of axonemal dynein Mdnah5 causes primary ciliary dyskinesia and hydrocephalus. Hum. Mol. Genet. **11:**715–721.
20. **Ihaka, R., and R. Gentleman.** 1996. A language for data analysis and graphics. J. Computat. Graph. Stat. **5:**299–314.
21. **Iwama, A., J. Pan, P. Zhang, W. Reith, B. Mach, D. G. Tenen, and Z. Sun.** 1999. Dimeric RFX proteins contribute to the activity and lineage specificity of the interleukin-5 receptor alpha promoter through activation and repression domains. Mol. Cell. Biol. **19:**3940–3950.

22. **Kobayashi, Y., M. Watanabe, Y. Okada, H. Sawa, H. Takai, M. Nakanishi, Y. Kawase, H. Suzuki, K. Nagashima, K. Ikeda, and N. Motoyama.** 2002. Hydrocephalus, situs inversus, chronic sinusitis, and male infertility in DNA polymerase lambda-deficient mice: possible implication for the pathogenesis of immotile cilia syndrome. Mol. Cell. Biol. **22:**2769–2776.
23. **Kozminski, K. G., K. A. Johnson, P. Forscher, and J. L. Rosenbaum.** 1993. A motility in the eukaryotic flagellum unrelated to flagellar beating. Proc. Natl. Acad. Sci. USA **90:**5519–5523.
24. **Lowe, L. A., S. Yamada, and M. R. Kuehn.** 2001. Genetic dissection of nodal function in patterning the mouse embryo. Development **128:**1831–1843.
25. **Marszalek, J. R., P. Ruiz-Lozano, E. Roberts, K. R. Chien, and L. S. Goldstein.** 1999. Situs inversus and embryonic ciliary morphogenesis defects in mouse mutants lacking the KIF3A subunit of kinesin-II. Proc. Natl. Acad. Sci. USA **96:**5043–5048.
26. **McGrath, J., and M. Brueckner.** 2003. Cilia are at the heart of vertebrate left-right asymmetry. Curr. Opin. Genet. Dev. **13:**385–392.
27. **McGrath, J., S. Somlo, S. Makova, X. Tian, and M. Brueckner.** 2003. Two populations of node monocilia initiate left-right asymmetry in the mouse. Cell **114:**61–73.
28. **Mikami, A., S. H. Tynan, T. Hama, K. Luby-Phelps, T. Saito, J. E. Crandall, J. C. Besharse, and R. B. Vallee.** 2002. Molecular structure of cytoplasmic dynein 2 and its distribution in neuronal and ciliated cells. J. Cell Sci. **115:**4801–4808.
29. **Murcia, N. S., W. G. Richards, B. K. Yoder, M. L. Mucenski, J. R. Dunlap, and R. P. Woychik.** 2000. The Oak Ridge polycystic kidney (orpk) disease gene is required for left-right axis determination. Development **127:**2347–2355.
30. **Nauli, S. M., F. J. Alenghat, Y. Luo, E. Williams, P. Vassilev, X. Li, A. E. Elia, W. Lu, E. M. Brown, S. J. Quinn, D. E. Ingber, and J. Zhou.** 2003. Polycystins 1 and 2 mediate mechanosensation in the primary cilium of kidney cells. Nat. Genet. **33:**129–137.
31. **Nonaka, S., H. Shiratori, Y. Saijoh, and H. Hamada.** 2002. Determination of left-right patterning of the mouse embryo by artificial nodal flow. Nature **418:**96–99.
32. **Nonaka, S., Y. Tanaka, Y. Okada, S. Takeda, A. Harada, Y. Kanai, M. Kido, and N. Hirokawa.** 1998. Randomization of left-right asymmetry due to loss of nodal cilia generating leftward flow of extraembryonic fluid in mice lacking KIF3B motor protein. Cell **95:**829–837.
33. **Norquay, L. D., X. Yang, P. Sheppard, S. Gregoire, J. G. Dodd, W. Reith, and P. A. Cattini.** 2003. RFX1 and NF-1 associate with P sequences of the human growth hormone locus in pituitary chromatin. Mol. Endocrinol. **17:**1027–1038.
34. **Okada, Y., S. Nonaka, Y. Tanaka, Y. Saijoh, H. Hamada, and N. Hirokawa.** 1999. Abnormal nodal flow precedes situs inversus in iv and inv mice. Mol. Cell **4:**459–468.
35. **Olbrich, H., K. Haffner, A. Kispert, A. Volkel, A. Volz, G. Sasmaz, R. Reinhardt, S. Hennig, H. Lehrach, N. Konietzko, M. Zariwala, P. G. Noone, M. Knowles, H. M. Mitchison, M. Meeks, E. M. Chung, F. Hildebrandt, R. Sudbrak, and H. Omran.** 2002. Mutations in DNAH5 cause primary ciliary dyskinesia and randomization of left-right asymmetry. Nat. Genet. **30:**143–144.
36. **Pazour, G. J., B. L. Dickert, Y. Vucica, E. S. Seeley, J. L. Rosenbaum, G. B. Witman, and D. G. Cole.** 2000. Chlamydomonas IFT88 and its mouse homologue, polycystic kidney disease gene tg737, are required for assembly of cilia and flagella. J. Cell Biol. **151:**709–718.
37. **Pazour, G. J., and J. L. Rosenbaum.** 2002. Intraflagellar transport and cilia-dependent diseases. Trends Cell Biol. **12:**551–555.
38. **Pennarun, G., E. Escudier, C. Chapelin, A. M. Bridoux, V. Cacheux, G. Roger, A. Clement, M. Goossens, S. Amselem, and B. Duriez.** 1999. Loss-of-function mutations in a human gene related to Chlamydomonas reinhardtii dynein IC78 result in primary ciliary dyskinesia. Am. J. Hum. Genet. **65:**1508–1519.
39. **Pennekamp, P., C. Karcher, A. Fischer, A. Schweickert, B. Skryabin, J. Horst, M. Blum, and B. Dworniczak.** 2002. The ion channel polycystin-2 is required for left-right axis determination in mice. Curr. Biol. **12:**938–943.
40. **Perrone, C. A., D. Tritschler, P. Taulman, R. Bower, B. K. Yoder, and M. E. Porter.** 2003. A novel dynein light intermediate chain co-localizes with the retrograde motor for intraflagellar transport at sites of axoneme assembly in Chlamydomonas and mammalian cells. Mol. Biol. Cell **14:**2041–2056.
41. **Qin, H., J. L. Rosenbaum, and M. M. Barr.** 2001. An autosomal recessive polycystic kidney disease gene homolog is involved in intraflagellar transport in C. elegans ciliated sensory neurons. Curr. Biol. **11:**457–461.
42. **Reith, W., C. Herrero-Sanchez, M. Kobr, P. Silacci, C. Berte, E. Barras, S. Fey, and B. Mach.** 1990. MHC class II regulatory factor RFX has a novel DNA binding domain and functionally independent dimerization domain. Genes Dev. **4:**1528–1540.
43. **Reith, W., and B. Mach.** 2001. The bare lymphocyte syndrome and the regulation of MHC expression. Annu. Rev. Immunol. **19:**331–373.
44. **Reith, W., C. Ucla, E. Barras, A. Gaud, B. Durand, C. Herrero-Sanchez, M. Kobr, and B. Mach.** 1994. RFX1, a transactivator of hepatitis B virus enhancer I, belongs to a novel family of homodimeric and heterodimeric DNA-binding proteins. Mol. Cell. Biol. **14:**1230–1244.
45. **Rosenbaum, J.** 2002. Intraflagellar transport. Curr. Biol. **12:**R125.
46. **Safrany, G., and R. P. Perry.** 1994. Transcription factor RFX1 helps control the promoter of the mouse ribosomal protein gene rpL30 by binding to its alpha element. Gene **132:**279–283.
47. **Samac, S., J. C. Rice, and M. Ehrlich.** 1998. Analysis of methylation in the 5′ region of the human alpha- galactosidase A gene containing a binding site for methylated DNA-binding protein/RFX1–4. Biol. Chem. **379:**541–544.
48. **Schafer, J. A., C. J. Haycraft, J. H. Thomas, B. K. Yoder, and P. Swoboda.** 2003. xbx-1 encodes a dynein light intermediate chain (DLIC) required for retrograde intraflagellar transport and cilia assembly in *C. elegans.* Mol. Biol. Cell **14:**2057–2070.
49. **Schaft, J., R. Ashery-Padan, F. van der Hoeven, P. Gruss, and A. F. Stewart.** 2001. Efficient FLP recombination in mouse ES cells and oocytes. Genesis **31:**6–10.
50. **Schwenk, F., U. Baron, and K. Rajewsky.** 1995. A cre-transgenic mouse strain for the ubiquitous deletion of loxP- flanked gene segments including deletion in germ cells. Nucleic Acids Res. **23:**5080–5081.
51. **Sengupta, P. K., J. Fargo, and B. D. Smith.** 2002. The RFX family interacts at the collagen (COL1A2) start site and represses transcription. J. Biol. Chem. **277:**24926–24937.
52. **Sloboda, R. D.** 2002. A healthy understanding of intraflagellar transport. Cell Motil. Cytoskeleton **52:**1–8.
53. **Steimle, V., B. Durand, E. Barras, M. Zufferey, M. R. Hadam, B. Mach, and W. Reith.** 1995. A novel DNA-binding regulatory factor is mutated in primary MHC class II deficiency (bare lymphocyte syndrome). Genes Dev. **9:**1021–1032.
54. **Supp, D. M., M. Brueckner, M. R. Kuehn, D. P. Witte, L. A. Lowe, J. McGrath, J. Corrales, and S. S. Potter.** 1999. Targeted deletion of the ATP binding domain of left-right dynein confirms its role in specifying development of left-right asymmetries. Development **126:**5495–5504.
55. **Swoboda, P., H. T. Adler, and J. H. Thomas.** 2000. The RFX-type transcription factor DAF-19 regulates sensory neuron cilium formation in C. elegans. Mol. Cell **5:**411–421.
56. **Theiler, K.** 1989. The house mouse. Development and normal stages from fertilization to 4 weeks of age. Springer-Verlag, Berlin, Germany.
57. **Torres, R. M., and R. Kuhn.** 1997. Laboratory protocols for conditional gene targeting. Oxford University Press, Oxford, United Kingdom.
58. **Venables, W. N., and B. B. Ripley.** 1999. Modern applied statistics with S-plus. Springer-Verlag, Berlin, Germany.
59. **Watanabe, D., Y. Saijoh, S. Nonaka, G. Sasaki, Y. Ikawa, T. Yokoyama, and H. Hamada.** 2003. The left-right determinant inversin is a component of node monocilia and other 9+0 cilia. Development **130:**1725–1734.
60. **Wilkinson, D. G.** 1992. Whole mount in situ hybridization of vertebrate embryos, p. 75–83. *In* E. D. G Wilkinson (ed.), In situ hybridization: a practical approach. IRL Press, Oxford, United Kingdom.
61. **Xu, G. M., S. Gonzalez-Perrett, M. Essafi, G. A. Timpanaro, N. Montalbetti, M. A. Arnaout, and H. F. Cantiello.** 2003. Polycystin-1 activates and stabilizes the polycystin-2 channel. J. Biol. Chem. **278:**1457–1462.